

# On Studying Charm in Nuclei through Antiproton Annihilation.

A. Sibirtsev<sup>1,2,a</sup>, K. Tsushima<sup>1,b</sup> and A. W. Thomas<sup>1,c</sup>

<sup>1</sup> Special Research Center for the Subatomic Structure of Matter (CSSM)  
 and Department of Physics and Mathematical Physics,  
 University of Adelaide, SA 5005, Australia

<sup>2</sup> Institut für Theoretische Physik, Universität Giessen,  
 D-35392 Giessen, Germany

Received: date / Revised version: date

**Abstract.** We examine the production of open charm in antiproton annihilation on finite nuclei. The enhancement of the subthreshold production cross section, even in a nucleus as light as carbon, should provide a clean signature of the reduction in the masses of these mesons in-medium. We also show that a careful analysis of the  $D^+$  and  $D^-$  spectra can yield important information on the cross section for  $D^\pm N$  scattering.

**PACS.** 25.43.+t Antiproton-induced reactions – 21.65.+f Nuclear matter – 14.40.Lb Charmed mesons – 14.65.Dw Charmed quarks

## 1 Introduction

Antiproton annihilation on nuclei provides new possibilities for studying open charm production, exploring the properties of charmed particles in nuclear matter and measuring the interaction of charmed hadrons.

Hatsuda and Kunihiro [1] proposed that the light quark condensates may be substantially reduced in hot and dense matter and that as a result hadron masses would be modified. At low density the ratio of the scalar hadron mass in medium to that in vacuum can be directly linked to the ratio of the quark condensates [2, 3, 4, 5, 6]. Even if the change in the ratio of the quark condensates is small, the absolute difference between the in-medium and vacuum masses of the hadron is expected to be larger for the heavy hadrons. In practice, any detection of the modification of the mass of a hadron in matter deals with the measurement of effect associated with this absolute difference.

It was found in Refs. [7, 8] that the in medium change of quark condensates is smaller for heavier quarks,  $s$  and  $c$ , than those for the light quarks,  $u$  and  $d$ . Thus the in-medium modification of the properties of heavy hadrons may be regarded as being controlled mainly by the light quark condensates. As a consequence we expect that charmed mesons, which consist of a light quark and heavy  $c$  quark, should serve as suitable probes of the in-medium modification of hadron properties.

As for the  $\bar{K}$  and  $K$ -mesons, with their quark contents  $\bar{q}s$  and  $q\bar{s}$  ( $q=u, d$  light quarks), respectively, the  $D$  ( $\bar{q}c$ ) and  $\bar{D}$  ( $q\bar{c}$ ) mesons will satisfy different dispersion relations in nuclear matter because of the different sign of the  $q$  and  $\bar{q}$  vector coupling. Some experimental confirmation of this effect has come from measurements [9, 10, 11, 12, 13, 14, 15, 16, 17] of  $K^-$  and  $K^+$ -meson production from heavy ion collisions. The  $D^+$  and  $D^-$  production from  $\bar{p}A$  annihilation might yield an even cleaner signal for the in-medium modification of the  $D$  and  $\bar{D}$  masses.

Because of charm conservation,  $D$  and  $\bar{D}$  mesons are produced pairwise and can be detected by their semileptonic decay channels. The threshold for the  $\bar{p}N \rightarrow D\bar{D}$  reaction in vacuum opens at an antiproton energy around 5.57 GeV, but it is lowered in the  $\bar{p}A$  annihilation by the in-medium modification of the  $D$  and  $\bar{D}$  masses as well as by Fermi motion.

The interaction of the  $D$ -mesons with nuclear matter is of special interest [18]. Note that the  $DN$  interaction should be very different from that of charmonia ( $J/\psi N$ ), since the interaction between the nucleons and the heavy mesons which do not contain  $u$  and  $d$  quarks is expected to proceed predominantly through gluon exchange. On the other hand, as for  $\bar{K}$ -mesons, the  $D$ -mesons might be strongly absorbed in matter because of the charm exchange reaction  $DN \rightarrow \Lambda_c \pi$ , while the  $\bar{D}$ -mesons should not be absorbed. As will be shown later, the specific conditions of the  $D\bar{D}$  pair production in  $\bar{p}A$  annihilation provide a very clean and almost model independent opportunity for the experimental reconstruction of the charm-exchange mechanism.

<sup>a</sup> alexandre.sibirtsev@theo.physik.uni-giessen.de

<sup>b</sup> ktsushim@physics.adelaide.edu.au

<sup>c</sup> athomas@physics.adelaide.edu.au

## 2 D-meson mass in nuclei

As far as the meson properties in free space are concerned, the Bethe-Salpeter (BS) and Dyson-Schwinger (DS) approaches have been widely used [19]. The application of BS approach to the description [20] of heavy and light quarks system allows well to describe the D and B meson properties in free space. The DS approach at finite baryon density was used [21] for the calculation of the in-medium properties of  $\rho$ ,  $\omega$  and  $\phi$  mesons. The modification of the  $\rho$  and  $\omega$  meson masses resulting from DS equation is close to the calculations with the quark-meson coupling (QMC) model [22], while the  $\phi$ -meson mass reduction from Ref. [21] is larger as compared to QMC. However, these approaches are not still developed well for the system of finite baryon density and we could not compare their results for the hadron properties in nuclear matter with the predictions from other models.

Here, we use the quark-meson coupling model [22], which has been successfully applied not only to the problems of conventional nuclear physics [23, 24] but also to the studies of meson properties in a nuclear medium [25, 26, 27]. Furthermore, the properties of the  $D$  meson (also  $B$ ) in free space are well described in an MIT bag model [28]. A detailed description of the Lagrangian density and the mean-field equations of motion needed to describe a finite nucleus are given in Refs. [23, 24]. At position  $\mathbf{r}$  in a nucleus (the coordinate origin is taken at the center of the nucleus), the Dirac equations for the quarks and antiquarks in the  $D$  and  $\bar{D}$  meson bags, neglecting the Coulomb force, are given by [25]:

$$\left[ i\gamma \cdot \partial_x - (m_q - V_\sigma^q(\mathbf{r})) \mp \gamma^0 \left( V_\omega^q(\mathbf{r}) + \frac{1}{2} V_\rho^q(\mathbf{r}) \right) \right] \times \begin{pmatrix} \psi_u(x) \\ \psi_{\bar{u}}(x) \end{pmatrix} = 0, \quad (1)$$

$$\left[ i\gamma \cdot \partial_x - (m_q - V_\sigma^q(\mathbf{r})) \mp \gamma^0 \left( V_\omega^q(\mathbf{r}) - \frac{1}{2} V_\rho^q(\mathbf{r}) \right) \right] \times \begin{pmatrix} \psi_d(x) \\ \psi_{\bar{d}}(x) \end{pmatrix} = 0, \quad (2)$$

$$[i\gamma \cdot \partial_x - m_c] \psi_c(x) \text{ (or } \psi_{\bar{c}}(x)) = 0. \quad (3)$$

The mean-field potentials for a bag centered at position  $\mathbf{r}$  in the nucleus are defined by  $V_\sigma^q(\mathbf{r}) = g_\sigma^q \sigma(\mathbf{r})$ ,  $V_\omega^q(\mathbf{r}) = g_\omega^q \omega(\mathbf{r})$  and  $V_\rho^q(\mathbf{r}) = g_\rho^q b(\mathbf{r})$ , with  $g_\sigma^q$ ,  $g_\omega^q$  and  $g_\rho^q$  the corresponding quark and meson-field coupling constants. (Note that we have neglected the small variation of the scalar and vector mean-fields inside the meson bag due to its finite size [23].) The mean meson fields are calculated self-consistently by solving Eqs. (23) – (30) of Ref. [24], namely, by solving a set of coupled non-linear differential equations for static, spherically symmetric nuclei, resulting from the variation of the effective Lagrangian density involving the quark degrees of freedom and the scalar, vector and Coulomb fields in mean field approximation.

The normalized, static solution for the ground state quarks or antiquarks in the meson bags may be written

as:

$$\psi_f(x) = N_f e^{-i\epsilon_f t / R_j^*} \psi_f(\mathbf{x}), \quad (j = D, \bar{D}), \quad (4)$$

where  $f = u, \bar{u}, d, \bar{d}, c, \bar{c}$  refers to quark flavors, and  $N_f$  and  $\psi_f(\mathbf{x})$  are the normalization factor and corresponding spin and spatial part of the wave function. The bag radius in medium,  $R_j^*$ , which generally depends on the hadron species to which the quarks and antiquarks belong, will be determined through the stability condition for the (in-medium) mass of the meson against the variation of the bag radius [23, 24, 25] (see also Eq. (9)). The eigenenergies  $\epsilon_f$  in Eq. (4) in units of  $1/R_j^*$  are given by

$$\begin{pmatrix} \epsilon_u(\mathbf{r}) \\ \epsilon_{\bar{u}}(\mathbf{r}) \end{pmatrix} = \Omega_q^*(\mathbf{r}) \pm R_j^* \left( V_\omega^q(\mathbf{r}) + \frac{1}{2} V_\rho^q(\mathbf{r}) \right), \quad (5)$$

$$\begin{pmatrix} \epsilon_d(\mathbf{r}) \\ \epsilon_{\bar{d}}(\mathbf{r}) \end{pmatrix} = \Omega_q^*(\mathbf{r}) \pm R_j^* \left( V_\omega^q(\mathbf{r}) - \frac{1}{2} V_\rho^q(\mathbf{r}) \right), \quad (6)$$

$$\epsilon_c(\mathbf{r}) = \epsilon_{\bar{c}}(\mathbf{r}) = \Omega_c(\mathbf{r}), \quad (7)$$

where  $\Omega_q^*(\mathbf{r}) = \sqrt{x_q^2 + (R_j^* m_q^*)^2}$ , with  $m_q^* = m_q - g_\sigma^q \sigma(\mathbf{r})$  and  $\Omega_c(\mathbf{r}) = \sqrt{x_c^2 + (R_j^* m_c)^2}$ . The bag eigenfrequencies,  $x_q$  and  $x_c$ , are determined by the usual, linear boundary condition [23, 24]. Note that the lowest eigenenergy for the Dirac equation (Hamiltonian) for the quark, which is positive, can be thought of (for many purposes) as a constituent quark mass.

Now, the  $D$  and  $\bar{D}$  meson masses in the nucleus at position  $\mathbf{r}$  (we take  $m_D = m_{\bar{D}}$  in vacuum, and then,  $m_D^* = m_{\bar{D}}^*$  in nuclear medium), are calculated by:

$$m_D^*(\mathbf{r}) = \frac{\Omega_q^*(\mathbf{r}) + \Omega_c(\mathbf{r}) - z_D}{R_D^*} + \frac{4}{3} \pi R_D^{*3} B, \quad (8)$$

$$\left. \frac{\partial m_D^*(\mathbf{r})}{\partial R_D} \right|_{R_D=R_D^*} = 0. \quad (9)$$

In Eq. (8), the  $z_j$  parametrize the sum of the center-of-mass and gluon fluctuation effects, and are assumed to be independent of density. The parameters are determined in free space to reproduce their physical masses.

In this study we chose the values  $m_q \equiv m_u = m_d = 5$  MeV and  $m_c = 1300$  MeV for the current quark masses, and  $R_N = 0.8$  fm for the bag radius of the nucleon in free space. Other input parameters and some of the quantities calculated are given in Refs. [23, 24, 25]. We stress that while the model has a number of parameters, only three of them,  $g_\sigma^q$ ,  $g_\omega^q$  and  $g_\rho^q$ , are adjusted to fit nuclear data – namely the saturation energy and density of symmetric nuclear matter and the bulk symmetry energy. None of the results for nuclear properties depend strongly on the choice of the other parameters – for example, the relatively weak dependence of the final results for the properties of finite nuclei, on the chosen values of the current quark mass and bag radius, is shown explicitly in Refs. [23, 24]. Exactly the same coupling constants,  $g_\sigma^q$ ,  $g_\omega^q$  and  $g_\rho^q$ , are used for the light quarks in the mesons as in the nucleon. However, in studies of the kaon system, we found that it was phenomenologically necessary to increase the strength of the vector

coupling to the non-strange quarks in the  $K^+$  (by a factor of  $1.4^2$ ) in order to reproduce the empirically extracted  $K^+$ -nucleus interaction [26,29]. We assume that the dynamical chiral symmetry breaking for the light quarks in the  $D$  and  $\bar{D}$  is the same as those for the kaon [25,26,29], and will use the stronger vector potential,  $\tilde{V}_\omega^q (= 1.4^2 V_\omega^q)$ , in this study.

Through Eqs. (1) – (9) we self-consistently calculate effective masses,  $m_D^*(\mathbf{r})$ , and mean field potentials,  $V_{\sigma,\omega,\rho}^q(\mathbf{r})$ , at position  $\mathbf{r}$  in the nucleus. The scalar and vector potentials (neglecting the Coulomb force) felt by the  $D$  and  $\bar{D}$  mesons, which depend only on the distance from the center of the nucleus,  $r = |\mathbf{r}|$ , are given by:

$$U_s^{D^\pm}(r) \equiv U_s(r) = m_D^*(r) - m_D, \quad (10)$$

$$U_v^{D^\pm}(r) = \mp(\tilde{V}_\omega^q(r) - \frac{1}{2}V_\rho^q(r)), \quad (11)$$

The  $\rho$  meson mean field potential,  $V_\rho^q(r)$ , (and the Coulomb potential) which are small and expected to give a minor effect, will be neglected in the present study. Note that  $V_\rho^q$  is negative in a nucleus with a neutron excess.

Fig.1 shows the potentials for the  $D^-$  and  $D^+$ -mesons as a function of the nuclear radius calculated for  $^{12}\text{C}$  and  $^{197}\text{Au}$ . For the following calculations we define the poten-

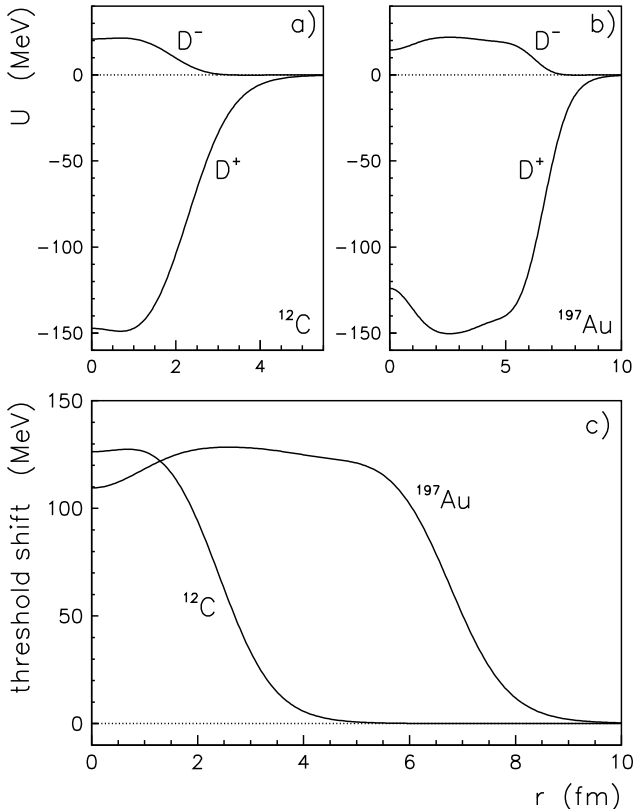


**Fig. 1.** The  $D^-$  and  $D^+$  potentials calculated for  $^{12}\text{C}$  (a) and  $^{197}\text{Au}$  (b) as a function of the nuclear radius. We also show the downward shift in the threshold for  $D^+D^-$  production for  $^{12}\text{C}$  and  $^{197}\text{Au}$ , in (c).

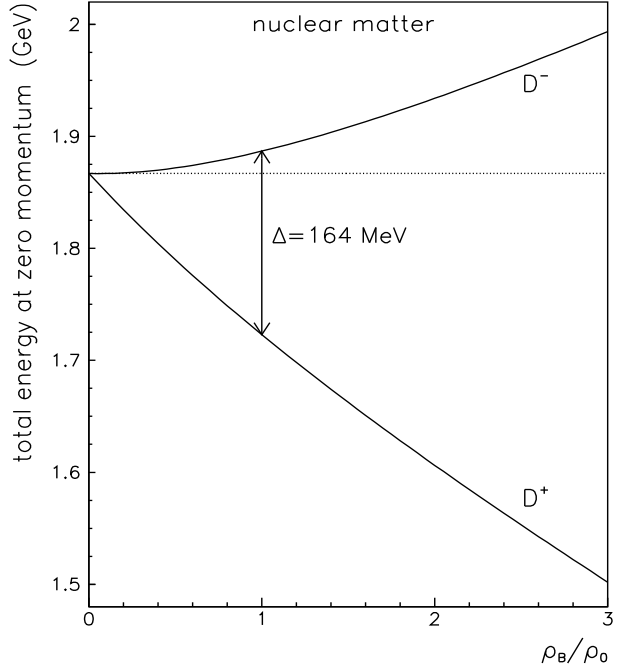


**Fig. 2.** The total energies of the  $D^-$  and  $D^+$  mesons at zero momentum calculated for nuclear matter and plotted as function of the baryon density, in units of the saturation density of nuclear matter,  $\rho_0 = 0.15 \text{ fm}^{-3}$ .

tial as

$$U^{D^\pm}(r) = U_s(r) + U_v^{D^\pm}(r), \quad (12)$$

where  $U_s$  and  $U_v$  denote the scalar and vector pieces of the potential, respectively. The in-medium dispersion relation, for the total energy  $E_{D^\pm}$  and the momentum  $p$  of the  $D^\pm$ -meson is now given by

$$E_{D^\pm}(\mathbf{r}) = \sqrt{p^2 + (m_D + U_s(r))^2} + U_v^{D^\pm}(r), \quad (13)$$

where the bare  $D$ -meson mass is  $m_D = 1.8693 \text{ GeV}$ .

Note that the total  $D^-$ -meson potential is repulsive, while the  $D^+$  potential is attractive, which is analogous to the case for the  $K^+$  and  $K^-$  mesons, respectively [26].

The amount of downward shift of the  $\bar{p}N \rightarrow D^+D^-$  reaction threshold in nuclei, associated with the in-medium modification of the  $D$  and  $\bar{D}$  scalar potentials and the vector potentials, is simply  $2U_s$ , and is shown in Fig.1c) for  $^{12}\text{C}$  and  $^{197}\text{Au}$  as a function of the nuclear radius. The threshold reduction is quite large in the central region of these nuclei and should be detected as an enhanced production of the  $D^+D^-$  pairs. Note that a similar situation holds for the  $K^+$  and  $K^-$  production and, indeed, enhanced  $K^-$ -meson production in heavy ion collisions, associated with the reduction of the production threshold, has been partially confirmed experimentally [9,10,11,12,13,14,15,16,17].

In Fig.2 the total energies of the  $D^+$  and  $D^-$  mesons at zero momentum in Eq. (13), are shown as function of the nuclear matter density in units of normal nuclear matter

density ( $\rho_0=0.15 \text{ fm}^{-3}$ ). Note that at  $\rho_0$  the threshold reduction is around 164 MeV, which should be detectable in  $\bar{p}A$  annihilation.

### 3 The model for D-meson production in $\bar{p}A$ annihilations

The  $D\bar{D}$  production in antiproton-nucleus annihilation was calculated using the cascade model [30] adopted for  $\bar{p}A$  simulations. The detailed description of the initialization procedure as well as the interaction algorithm are given in Ref. [30].

The reaction zone was initialized with the use of the momentum dependent  $\bar{p}N$  total cross section, given as [31]:

$$\sigma_{\bar{p}N} = 38.4 + 77.6p^{-0.64} + 0.26(\ln p)^2 - 1.2 \ln p, \quad (14)$$

where  $p$  denotes the antiproton laboratory momentum and the cross section was taken to be the same for the proton and the neutron target (in good agreement with the data [31]).

The  $\bar{p}N \rightarrow D\bar{D}$  cross section was calculated with quark-gluon string model proposed in Ref. [32]. In the following we will concentrate on the production of  $D^+$  and  $D^-$ -mesons and thus take into account only two possible reactions, namely  $\bar{p}p \rightarrow D^+D^-$  and  $\bar{p}n \rightarrow D^0D^-$ . Note that the relation,

$$4\sigma(\bar{p}p \rightarrow D^+D^-) = \sigma(\bar{p}n \rightarrow D^0D^-) \quad (15)$$

is due to the difference in the number of the quark planar diagrams [32].

Furthermore, to account for the  $D^-$  and  $D^+$ -meson propagation in nuclear matter one needs to introduce the relevant cross sections for elastic and inelastic  $DN$  scattering. Since no data for the  $DN$  interaction are available we use a diagrammatic approach illustrated by Fig.3a,b). Let us compare the  $D^-N \rightarrow D^-N$  and the  $K^+N \rightarrow K^+N$  reactions in terms of the quark lines. Apart from the difference between the  $c$  and  $s$  quarks, both reactions are very similar and can be understood in terms of rearrangement of the  $u$  or  $d$  quarks. Thus, in the following calculations we assume that  $\sigma_{D^-N \rightarrow D^-N} = \sigma_{K^+N \rightarrow K^+N}$ .

The  $K^+N$  cross section was taken from Ref.[33], which gives a parametrization of the available experimental data. The total  $K^+N$  cross section, averaged over neutron and proton targets, is shown in Fig.4a) by the dashed line - as a function of the kaon momentum in the laboratory system. Note, that within a wide range of kaon momentum  $\sigma_{K^+N}$  is almost constant and approaches a value of  $\simeq 20$  mb. We adopt the value  $\sigma_{D^-N} = 20$  mb, noting that it is entirely due to the elastic scattering channel.

Now, Fig.3c,d) shows both the  $K^-N \rightarrow \Lambda\pi$  and  $D^+N \rightarrow \Lambda_c\pi$  processes, which are again quite similar in terms of the rearrangement of the  $s$  and  $c$  quarks, respectively. Thus we assume that  $\sigma_{D^+N \rightarrow \Lambda_c\pi} \simeq \sigma_{K^-N \rightarrow \Lambda\pi}$ .

The total  $K^-N$  cross section is shown by the solid line in Fig.4. Again it is averaged over proton and the

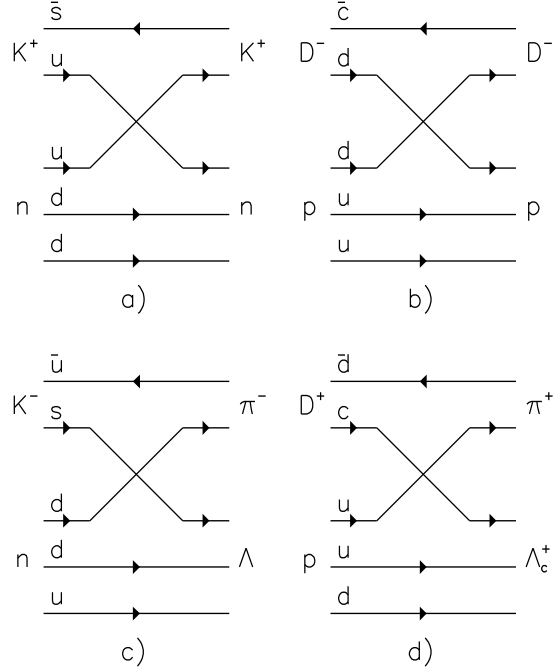


**Fig. 3.** Quark diagrams for  $K^+n \rightarrow K^+n$  (a) and  $D^-p \rightarrow D^-p$  (b) elastic scattering and for  $K^-n \rightarrow \Lambda\pi^-$  (c),  $D^+p \rightarrow \Lambda_c^+\pi^+$  (d) inelastic scattering.

neutron and taken as a parametrization [33] of the experimental data. At low momenta the  $K^-N$  cross section shows resonance structures due to the strange baryonic resonances [34], while at high momenta it approaches a constant value. Apart from the contribution from these intermediate baryonic resonances the inelastic  $K^-N \rightarrow \Lambda\pi$  cross section can be written as

$$\sigma_{K^-N \rightarrow \Lambda\pi} = \frac{|M|^2}{16\pi s} \times \left[ \frac{(s - m_A^2 - m_\pi^2)^2 - 4m_A^2 m_\pi^2}{(s - m_K^2 - m_N^2)^2 - 4m_N^2 m_K^2} \right]^{1/2}, \quad (16)$$

where  $s$  is the square of the invariant collision energy and  $m_K$ ,  $m_N$ ,  $m_\Lambda$ ,  $m_\pi$  are the masses of kaon, nucleon,  $\Lambda$ -hyperon and pion, respectively. In Eq.(16) the  $|M|$  denotes the matrix element of the  $K^-N \rightarrow \Lambda\pi$  transition, which was taken as a constant. Now the total  $K^-N$  cross section is given as a sum of the cross section for the inelastic channel (16) and for the elastic one, where the latter was taken to be 20.5 mb. The dotted line in Fig.4 shows our result for the total  $K^-N$  cross section obtained with  $|M|=11.64 \text{ GeV}\cdot\text{fm}$ , which reproduces the trend of the data reasonably well.

A similar approach was used to construct the  $D^+N$  total cross section. It was assumed that at high momenta the  $D^+N$  elastic cross section equals the  $D^-N$  cross section, while the  $D^+N \rightarrow \Lambda_c^+\pi$  cross section was calculated from Eq.16, replacing the particle masses as appropriate.

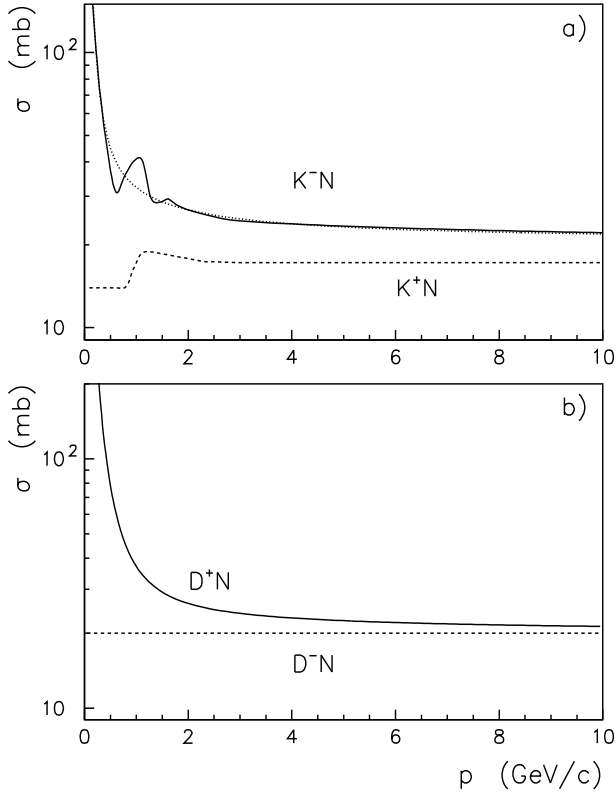


**Fig. 4.** a) The total  $K^-N$  (solid) and  $K^+N$  (dashed line) cross sections obtained [33] as the best fit to the available experimental data [34] and shown as function of the kaon momentum. The dotted line show the result as explained in the text. b) The  $D^+N$  (solid) and  $D^-N$  total cross sections used in the calculations.

The final results are shown in Fig.4 and were adopted for the following calculations.

We wish to emphasize that the status of the  $D$ -meson-nucleon interactions is still unknown and is itself one of the important goals of the  $\bar{p}A \rightarrow DD\bar{X}$  studies. Our approach is necessary in order to estimate the expected sensitivity of the experimental measurements to the  $DN$  interaction and to study the possibility to evaluate the  $D^+N$  and  $D^-N$  cross sections.

#### 4 Testing the D-mass in matter

In comparison to low energy antiprotons that annihilate at the periphery of the nucleus because of the large  $\bar{p}N$  annihilation probability, antiprotons with energies above 3 GeV should penetrate the nuclear interior. They can therefore probe the nuclear medium at normal baryon density  $\rho_0$  and hence yield information about the in-medium properties of the particles. Indeed, as is illustrated by Fig.1, the  $D$ -meson potential deviates strongly from zero in the interior of the nuclei considered.

Fig.5 shows the reaction zone for the  $\bar{p}C$  and  $\bar{p}Au$  annihilations at an antiproton beam energy of 5 GeV. The

plots are given as a functions of the impact parameter  $b$  and the  $z$ -coordinate, assuming the beam is oriented along the  $z$ -axis, which is shown by arrows in Fig.5. The annihilation zone is concentrated in the front hemisphere of the target nuclei. Actually the antiprotons penetrate sufficiently deeply to test densities near that of normal nuclear matter and hence the shift in the  $D^+D^-$  production threshold should be manifest.

Now we calculate the total  $\bar{p}A \rightarrow D^+D^-X$  production cross section as function of the antiproton beam energy and show the results in Fig.6 for a carbon target and in Fig.7 for gold. The vacuum  $\bar{p}N \rightarrow D^+D^-$  cross section is also shown in Fig.7. Note that the difference between the  $D^+$  and  $D^-$ -meson production rates is caused by the  $D^+$ -absorption in nuclear matter.

Obviously the production threshold is substantially reduced as compared to the antiproton annihilation on a free nucleon. Apparently, part of this reduction is due to the Fermi motion [35,36,37], however the calculations with in-medium  $D$ -meson masses indicate a much stronger threshold reduction comparing to those using the free masses for the final  $D$ -mesons.

Note that, because of their relatively long mean life, the  $D$ -mesons decay outside the nucleus and their in-

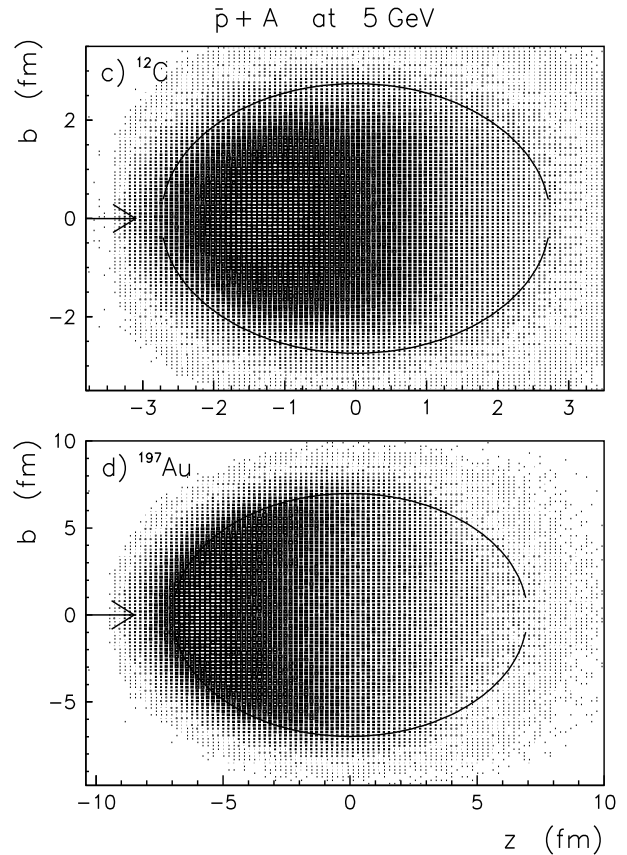


**Fig. 5.** The plot of the annihilation zone for  $\bar{p}+^{12}C$  (a) and  $\bar{p}+^{197}Au$  (b) reactions at a beam energy of 5 GeV. The solid line indicates the r.m.s. radius of the target nucleus. The arrows show the direction of the antiproton beam.

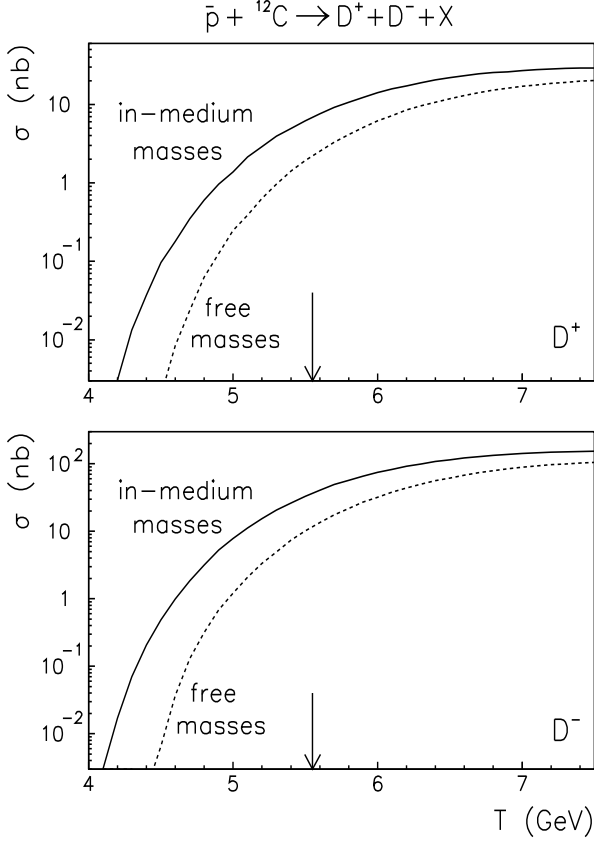


**Fig. 6.** The total cross section for  $D^+$  and  $D^-$ -meson production in  $\bar{p}C$  annihilation as a function of the antiproton energy. The results are shown for calculations with free (dashed lines) and in-medium masses (solid lines) for the  $D$ -mesons. The arrow indicates the reaction threshold on a free nucleon.

medium masses cannot be detected through a shift of the invariant mass of the decay products (unlike the leptonic decay of the vector mesons). Thus it seems that the modification of the  $D^+$  and  $D^-$ -meson masses in nuclear matter can best be detected experimentally as for the shift of the in-medium  $K^+$  and  $K^-$ -meson masses, namely as an enhanced  $D$ -meson production rate at energies below the threshold for the  $\bar{p}N \rightarrow D^+D^-$  reaction in free space.

We should note that experimentally it may be difficult to distinguish whether such an enhancement is due to the modification of the  $D^+$  and  $D^-$ -meson masses in nuclear matter, or due to the Fermi motion, or due to other processes that are not yet included in our study. In principle, the high momentum component of the nuclear spectral function can provide sufficient energy for particle production far below the reaction threshold in free space [35]. However, the calculations in Refs. [36,37] with realistic spectral functions [39,40,41] indicate that such effects are actually negligible, while a more important contribution comes from multistep production mechanism. For instance, the dominant contribution to  $K^+$  production in  $pA$  collisions comes from the secondary  $\pi N \rightarrow YK^+$  process, which prevails over the direct  $pN \rightarrow NYK^+$  reaction

mechanism [36,38]. Thus the interpretation of the data depends substantially on the reliable measurement of the production mechanism.

It is important, that an additional advantage of the  $D^+D^-$  production in  $\bar{p}A$  annihilation is the possibility to reconstruct the production mechanism directly. Let us denote as  $M_X$  the missing mass of the target nucleon in the reaction  $\bar{p}N \rightarrow D^+D^-$ . Obviously, in vacuum  $M_X$  is equal to the free nucleon mass and can be reconstructed for antiproton energies above the  $D^+D^-$  production threshold on the free nucleon. When analysing  $M_X$  in  $\bar{p}A$  annihilations one expects the distribution  $d\sigma/dM_X$  to be centered close to the mass of the bound nucleon - below the free nucleon mass. The shape of the distribution  $d\sigma/dM_X$  is related to the spectral function of the nucleus [39,40,41].

The preceding discussion is based on the hypothesis that the reaction  $\bar{p}N \rightarrow D^+D^-$  is the dominant mechanism for  $D^+D^-$  pair production. By measuring both the  $D^+$  and  $D^-$  mesons one can directly check this hypothesis.

Let us first neglect the  $D$ -meson interactions in the nuclear environment and analyze the  $M_X$  spectrum for  $\bar{p}C$  annihilation at 5 GeV. Fig.8a) shows the missing mass distribution calculated without (hatched histogram) and with inclusion of the  $D^+$  and  $D^-$ -meson potentials. We recall

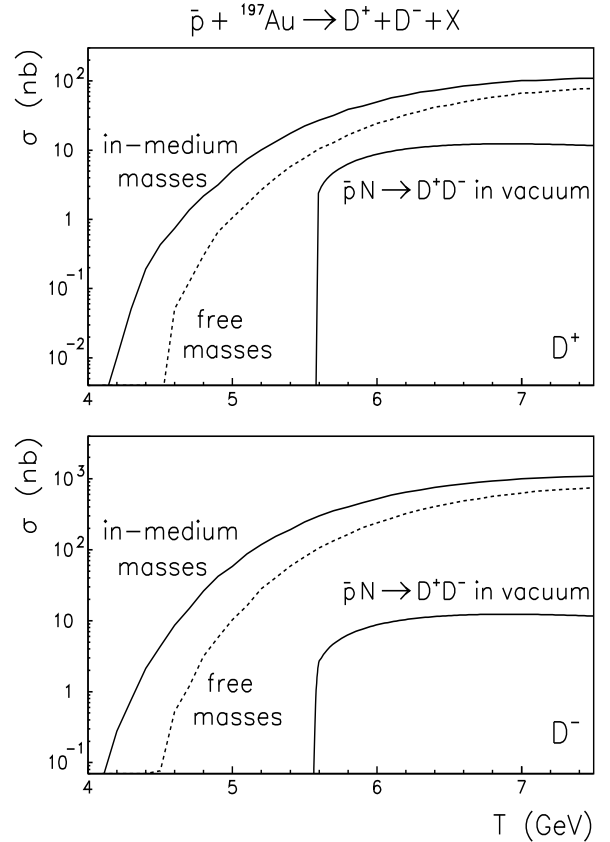


**Fig. 7.** The total cross section for  $D^+$  and  $D^-$ -meson production in  $\bar{p}Au$  annihilation as function of the antiproton energy. The results are shown for calculations with free (dashed lines) and in-medium masses (solid lines) for the  $D$ -mesons. For comparison the vacuum  $\bar{p}N \rightarrow D^+D^-$  cross section is also indicated.

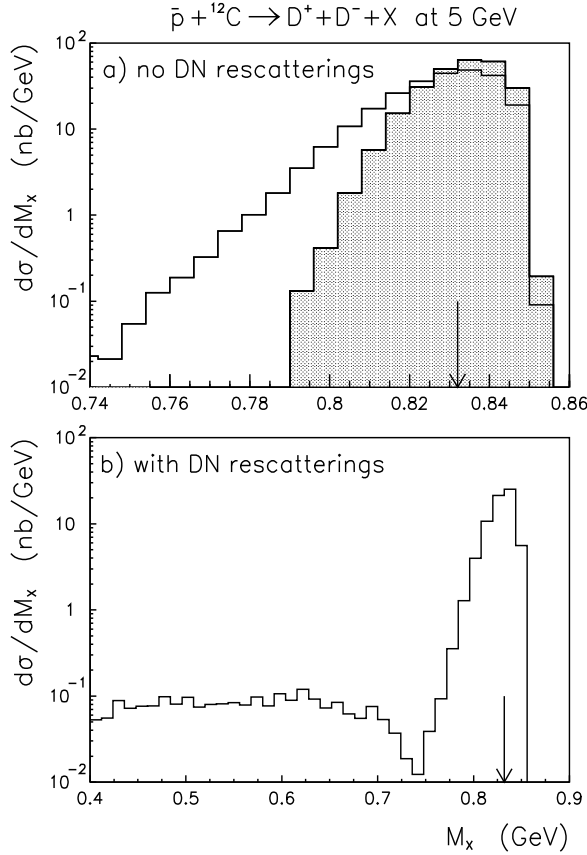


**Fig. 8.** The missing mass distribution calculated for  $\bar{p}C$  annihilation at 5 GeV. The upper part shows the results obtained without (hatched histogram) and with account of the in-medium potentials (open histogram), but neglecting the  $D$ -meson interactions in the nucleus. The hatched histogram is normalized to the open histogram. The lower part shows the calculations with  $D^+$  and  $D^-$  potentials and with  $DN$  interactions.

that calculations with free masses provide much smaller  $\bar{p}C \rightarrow D^+ D^- X$  production cross sections (see Fig.6). Thus, for the purpose of the comparison in Fig.8a) the result obtained without potentials is renormalized to those with in-medium masses.

The arrow in Fig.8a) indicates the density averaged mass of the bound nucleon in the carbon target [42]. Indeed both histograms are centered around the expected value. However, the calculation with the potentials shows a substantially wider distribution. This effect can be easily understood in terms of the downward shift of the threshold for  $D$ -meson production in medium.

Fig.8b) shows the  $M_X$  distribution calculated with in-medium masses, taking into account both  $D^+$  and  $D^-$ -meson interactions in the nuclear environment. Note that the distribution below  $M_X \simeq 0.75$  GeV results from secondary  $DN$  elastic rescattering and its strength is proportional to the  $DN$  elastic cross section. A deviation of the actual experimental missing mass distribution from those shown in Fig.8b) might directly indicate the con-

tribution from  $D^+ D^-$  reaction mechanisms, other than direct production.

In principle, the missing mass,  $M_X$ , reconstruction appears as a very promising tool for the detection of the in-medium mass modification. Of course, this method requires a detailed knowledge of the nuclear spectral function [39,40,41] as well as an accurate calculation of the  $M_X$  distribution, which should be compared to the experimental one.

## 5 Determination of the $DN$ cross section

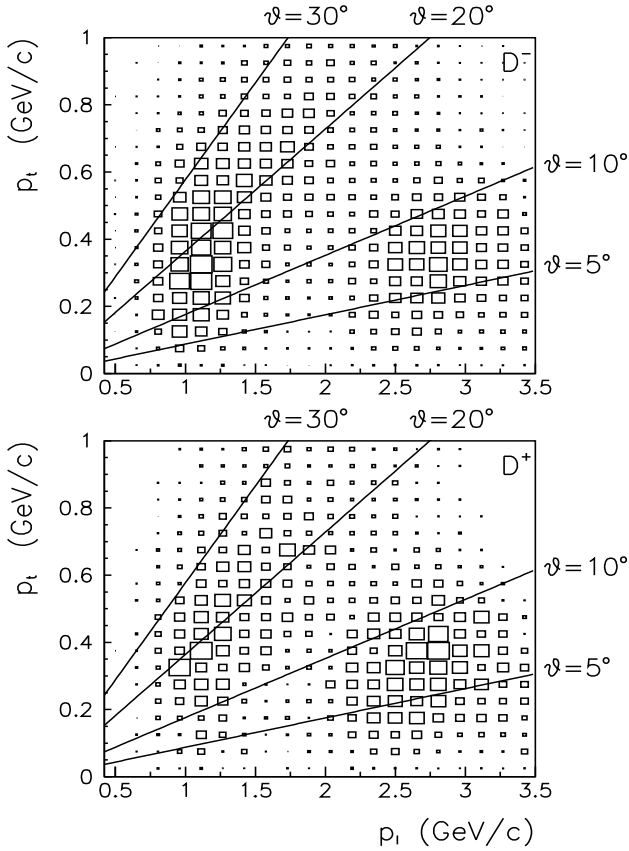
Obviously both  $D^+$  and  $D^-$  mesons are produced in the fragmentation region of the incident antiproton. The  $D^+ D^-$  pairs gain the total energy available from the  $\bar{p}N$  annihilation and because of the high velocity of the antiproton beam they should move forward with large momenta - at least when the produced mesons do not interact with the target.

Fig.9 shows the  $D^+$  and  $D^-$ -meson distribution in momentum space, i.e. over the transverse momentum  $p_t$ , and laboratory, longitudinal momentum,  $p_l$ , calculated for the  $\bar{p}Au$  reaction at an antiproton energy of 7 GeV. The solid lines indicate the  $D$ -meson emission angle in the laboratory system. The  $D$ -meson distribution in momentum space shows two branches. The branch at large  $p_l$  and small  $p_t$  originates from the primary production of the  $D^+ D^-$  pairs in the antiproton annihilation at the target nuclei. The width of this branch reflects the spectral function of the nuclei, i.e. the internal momentum and energy distribution of the nucleons [39,40,41].

The second branch in Fig.9 is located at small  $p_l$  and originates from the elastic and inelastic interactions of the  $D$ -meson in nuclear medium. Note that the  $D^+$  mesons are produced in the annihilation with sufficiently large momenta that they are not strongly absorbed (see Fig.4) but can be scattered elastically similar to the  $D^-$ -mesons. Obviously, to be absorbed the  $D^+$ -mesons should first be slowed down in the nuclear matter. Thus the experimental study of the charm exchange reaction,  $D^+ N \rightarrow \Lambda_c^+ \pi$ , seems to be more informative with the heavy nuclear targets, where multiple scattering is more probable.

The momentum spectra for  $D^-$  and  $D^+$ -mesons produced in  $\bar{p}C$  annihilation at 5 GeV are shown in Fig.10. The hatched histograms are the primary spectra from  $\bar{p}$ -annihilation on the target nucleon, while the solid histograms show the final  $D$ -meson spectra. The difference between the primary and final spectra arise primary from elastic rescattering. For such a light target as carbon, the  $D^+$ -absorption is almost negligible and therefore the difference between the  $D^-$  and  $D^+$  momentum spectra is only the absolute normalization. Note that the  $D^+$  can be produced in  $\bar{p}$  annihilation at the target proton, while  $D^-$  - can be produced on either a neutron or proton.

A rather different situation applies for the antiproton annihilation on heavy targets. Fig.11 shows the  $D$ -meson spectra from  $\bar{p}Au$  annihilations at 5 GeV. Again the hatched histograms are the primary spectra from the annihilation, while the solid histograms show the final spec-



**Fig. 9.** The distribution over the transverse  $p_t$  and laboratory longitudinal momentum  $p_l$  for the  $D^-$  (upper part) and  $D^+$ -meson (lower part) produced in  $\bar{p}Au$  annihilations at 7 GeV. Lines indicate the detection angle in the laboratory system.

tra. The  $D^-$ -meson spectrum is enhanced at low momenta which indicates strong  $D^-$  deceleration in the gold. At the same time the total  $D^-$  yield does not change in comparison with the primary production.

The  $D^+$ -spectrum is substantially different from the primary (shadowed histogram) and around 40% of the initial  $D^+$ -mesons, produced in  $\bar{p}Au$  annihilation at 5 GeV, are absorbed. Indeed the difference between the  $D^+$  and  $D^-$  spectra comes from the  $D$ -nucleon absorption.

## 6 Conclusion

We have studied  $D$ -meson production in antiproton-nucleus annihilation. It was found that  $\bar{p}A$  annihilation at energies below the  $\bar{p}N \rightarrow D^+ D^-$  reaction threshold in free space offer reasonable conditions for the detection of the changes in  $D$ -meson properties in-medium at normal nuclear matter density. In-medium modification of the  $D$ -meson mass can be observed as an enhanced  $D^+ D^-$  production at antiproton energies below  $\simeq 5.5$  GeV. The advantage of the  $\bar{p}A \rightarrow D^+ D^- X$  reaction is the possibility to reconstruct directly the primary production mechanism and hence to avoid a mistaken interpretation of such an enhancement as due to the contribution from multistep production processes. In part this reconstruction allows one to restrict

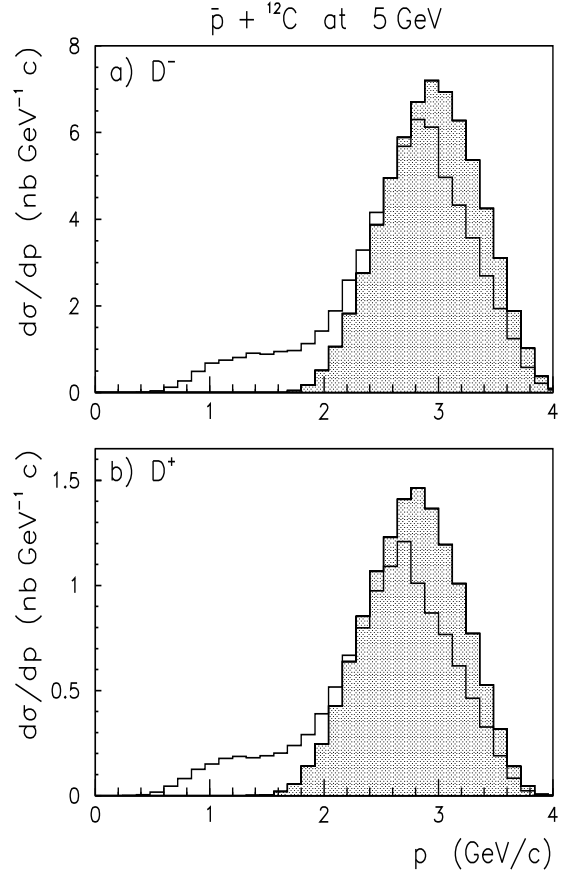


**Fig. 10.** The momentum spectra of  $D^-$  and  $D^+$  mesons in the laboratory system and from the  $\bar{p}C$  annihilations at 5 GeV. Hatched histograms show the primary spectra from the antiproton annihilation at the bound nucleon. Solid histograms are the final spectra.

the data analysis in terms of the effect due to the high momentum component of the nuclear spectral function. The study of the in-medium modification of the  $D$ -meson mass seems very promising, even with a target as light as carbon, where the total  $D^+ D^-$  mass reduction is sizeable and the nuclear spectral function is under control [39, 40, 41].

We found that the  $\bar{p}A$  annihilations also provide favourable conditions for studying the  $D$ -meson interaction in the nucleus. The difference in the  $D^+$  and  $D^-$ -meson momentum spectra from antiproton annihilation on heavy nuclei provides a very clean signature for the charm exchange  $D^+ N \rightarrow \Lambda_c^+ \pi$  reaction and can be used for the determination of the  $DN$  rescattering and absorption cross sections.

A.S would like to acknowledge the warm hospitality and partial support of the CSSM. This work was supported by the Australian Research Council and the Forschungszentrum Jülich.

## References

1. Hatsuda, T., Kunihiro, T.: Phys. Rev. Lett. **55**, (1985) 158; Phys. Rep. **247**, (1994) 221.
2. Nelson, A.E., Kaplan, D.B.: Phys. Lett. **B192**, (1987) 193.
3. Brown, G.E., Kubodera, K.: Rho, M.: Phys. Lett. **B192**, (1987) 273.
4. Hatsuda, T., Lee, S.H.: Phys. Rev. **C46**, (1992) R34.
5. Lutz, M., Steiner, A., Weise, W.: **A574**, (1994) 755.
6. Saito, K., Thomas, A.W.: Phys. Rev. **C51**, (1995) 2757.
7. Klingl, F., Kim, S., Lee, S.H., Morath, P., Weise, W.: Phys. Rev. Lett. **82**, (1999) 3396.
8. Hayashigaki, A.: nucl-th/9811092.
9. Laue, F., et al.: Phys. Rev. Lett. **82**, (1999) 1640.
10. Schroter, A., et al.: Z. Phys. **A350**, (1994) 101.
11. Ritman, J.L., et al.: Z. Phys. **A352**, (1995) 355.
12. Barth, R., et al.: Phys. Rev. Lett. **78**, (1997) 4007.
13. Shin, Y., et al.: Phys. Rev. Lett. **81**, (1998) 1576.
14. Li, G.Q., Ko, C.M., Fang, X.S.: Phys. Lett. **B329**, (1994) 149.
15. Cassing, W., Bratkovskaya, E.L., Mosel, U., Teis, S., Sibirtsev, A.: Nucl. Phys. **A614**, (1997) 415.
16. Li, G.Q., Ko, C.M., Brown, G.E.: Phys. Lett. **B381**, (1996) 17.
17. Cassing, W., Bratkovskaya, E.L.: Phys. Rep. **308**, (1999) 65.
18. Kharzeev, D.E.: Sov. J. Nucl. Phys. **51**, (1990) 185; Nucl. Phys. **A558**, (1993) 331c; Sov. J. Nucl. Phys. **55**, (1992) 746.

19. For example, Miransky, V.A.: *Dynamical Symmetry Breaking in Quantum Field Theories*, World Scientific Publishing Co., (1993).
20. Kalinovsky, Yu.L., Weiss, C.: Z. Phys. **C63**, (1994) 275.
21. Blaschke, D., Roberts, C.D.: Nucl. Phys. **A642**, (1998) 197.
22. Guichon, P.A.M.: Phys. Lett. **B200**, (1998) 235.
23. Guichon, P.A.M., Saito, K., Rodionov, E., Thomas, A.W.: Nucl. Phys. **A601**, (1996), 349
24. Saito, K., Tsushima, K., Thomas, A.W.: Nucl. Phys. **A609**, (1996) 339.
25. Tsushima, K., Lu, D.H., A.W. Thomas, Saito, K., Landau, R.H.: Phys. Rev. **C59**, (1999) 2824; Tsushima, K.: ADP-98-73/T340, nucl-th/9811063; ADP-99-7/T352, nucl-th/9901095.
26. Tsushima, K., Saito, K., Thomas, A.W., Wright, S.W.: Phys. Lett. **B429**, (1998) 239; *ibid.* **B436**, (1998), 453.
27. For recent results of QMC, Thomas, A.W., Lu, D.H., Tsushima, K., Williams, A.G., Saito, K.: nucl-th/9807027, to be published in the proceedings of the TJNAF Users Workshop.
28. Sadzikowski, M.: Z. Phys. C **C67**, (1995) 129.
29. Waas, T., Weise, W.: Nucl. Phys. **A625**, (1997) 287; Waas, T., Kaiser, N., Weise, W.: Phys. Lett. **B379**, (1996) 34.
30. Sibirtsev, A.: Sov. J. Nucl. Phys. **54**, (1991) 426; Sibirtsev, A., Armstrong, T.A., Lam, C., Lewis, R.A., Minor, E.D., Smith, G.: Z. Phys. **A347**, (1994) 277; Buescher, M., Sibirtsev, A., Sistemich, K.: Z. Phys. **A350**, (1994), 161; Sibirtsev, A.: Z. Phys. **A350**, (1994) 269; Acta Phys. Polon. **B24**, (1994) 1849; Z. Phys. A **345**, (1993) 59; Sov. J. Nucl. Phys. **55**, (1992) 729.
31. Particle Data Group, Phys. Rev. **D50**, (1994) 1335.
32. Kaidalov, A.B., Volkovitsky, P.E.: Z. Phys. **C63**, (1994) 517.
33. Sibirtsev, A., Cassing, W.: Nucl. Phys. **A641**, (1998), 476.
34. Particle Data Group, Eur. Phys. J. **C3**, (1998) 1.
35. Sibirtsev, A.: Phys. Lett. **B359**, (1995) 29.
36. Debowski, M. et al., Z. Phys. **A356**, (1996) 313.
37. Sibirtsev, A., Cassing, W., Mosel, U.: Z. Phys. **A358**, (1997) 357.
38. Badala, A., et al.: Phys. Rev. Lett. **80**, (1998) 4863.
39. Benhar, O., A. Fabrocini, A., Fantoni, S.: Nucl. Phys. **A505**, (1989) 267.
40. Sick, I., S. Fantoni, S., Fabrocini, A.: Phys. Lett. **B323**, (1994) 267.
41. Ciofi degli Atti, C., Simula, S.: Phys. Rev. **C53**, (1996) 1689.
42. Saito, K., Tsushima, K., Thomas, A.W.: Phys. Rev. **C56**, (1997) 566.

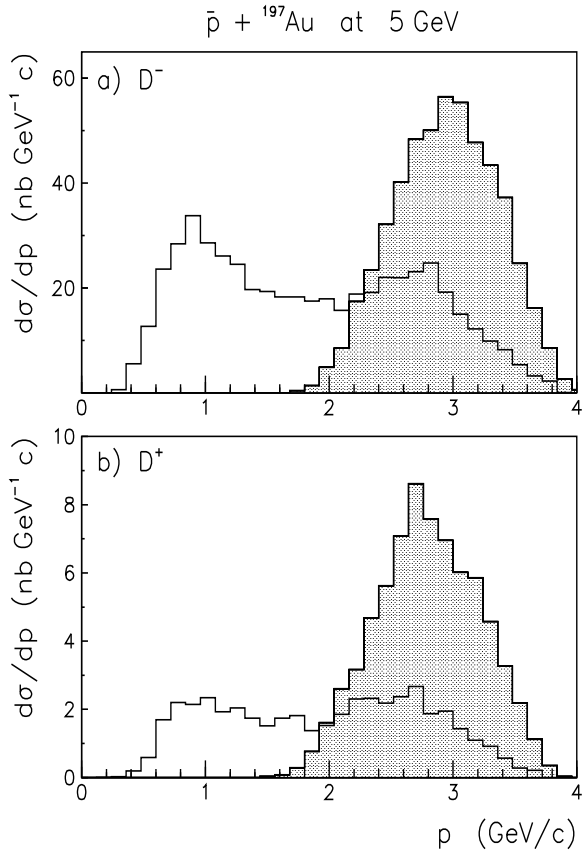


**Fig. 11.** The momentum spectra of  $D^-$  and  $D^+$  mesons in the laboratory system and from the  $\bar{p}Au$  annihilations at 5 GeV. Hatched histograms show the primary spectra from the antiproton annihilation at the bound nucleon. Solid histograms are the final spectra.